Fringe Modulation Characterization for a Phase Shifting Imaging Ellipsometer

Conrad Wells[a] and James C. Wyant[a,b]

[a]Optical Sciences Center, University of Arizona, Tucson, AZ 85721-0094
[b]WYKO Corporation, 2650 East Elvira Road, Tucson, AZ 85706-7123

Abstract

An imaging ellipsometer has been developed which employs phase shifting interferometry to characterize the ellipsometeric parameters. A modified Michelson interferometer is used in conjunction with a Wollaston prism to generate two interferograms with orthogonal polarization states. Subtraction of the phases in the two interferograms yields the ellipsometeric parameter Δ. The fringe modulation of the two interferograms is used to calculate the ellipsometeric parameter Ψ. The characterization of the average intensity of the interferogram is the largest contributor to the errors in the modulation. New algorithms for reducing the errors in modulation calculations for phase shifting interferometry are presented. The design of the instrument, results of measurements and algorithms for modulation characterization will be presented.

Keywords: Ellipsometry, Interferometeric Ellipsometry, Thin Films, Phase Shifting Interferometry, Imaging Ellipsometer, Visibility, Modulation

1. Introduction

Many authors have designed and tested interferometric ellipsometers[1-2]. In addition, imaging ellipsometers[3-4] based on conventional ellipsometeric techniques have been developed. The impetus of this work is the development of an imaging ellipsometer employing phase shifting interferometry to characterize the ellipsometeric parameters. A number of novel layouts were identified, but the layout in figure 1 was chosen for the building of a prototype.

2. Theory and Instrument Layout

Figure 1 illustrates the layout of the instrument. A light source is collimated and directed through a polarizer oriented at 45 degrees. This source can be a laser or an incoherent source such as an LED. The light is then reflected off the sample of interest before passing into a modified Michelson interferometer. The Jones matrix for the light hitting the sample and entering the interferometer are

$$E_{source} = \begin{bmatrix} 1 \\ 1 \end{bmatrix} \quad \text{Eq. 1}$$

$$E_{Interferometer\ Input} = \begin{bmatrix} \rho_s \\ \rho_p \end{bmatrix} \quad \text{Eq.2}$$

Where $\rho_s = |\rho_s| e^{i\Phi_s}$ and $\rho_p = |\rho_p| e^{i\Phi_p}$ are the complex amplitude reflection coefficients for the object of interest. All subsequent references to reflectance will refer to the complex amplitude reflection. Since this ellipsometer is imaging a two dimensional region, the phases are a function of position.

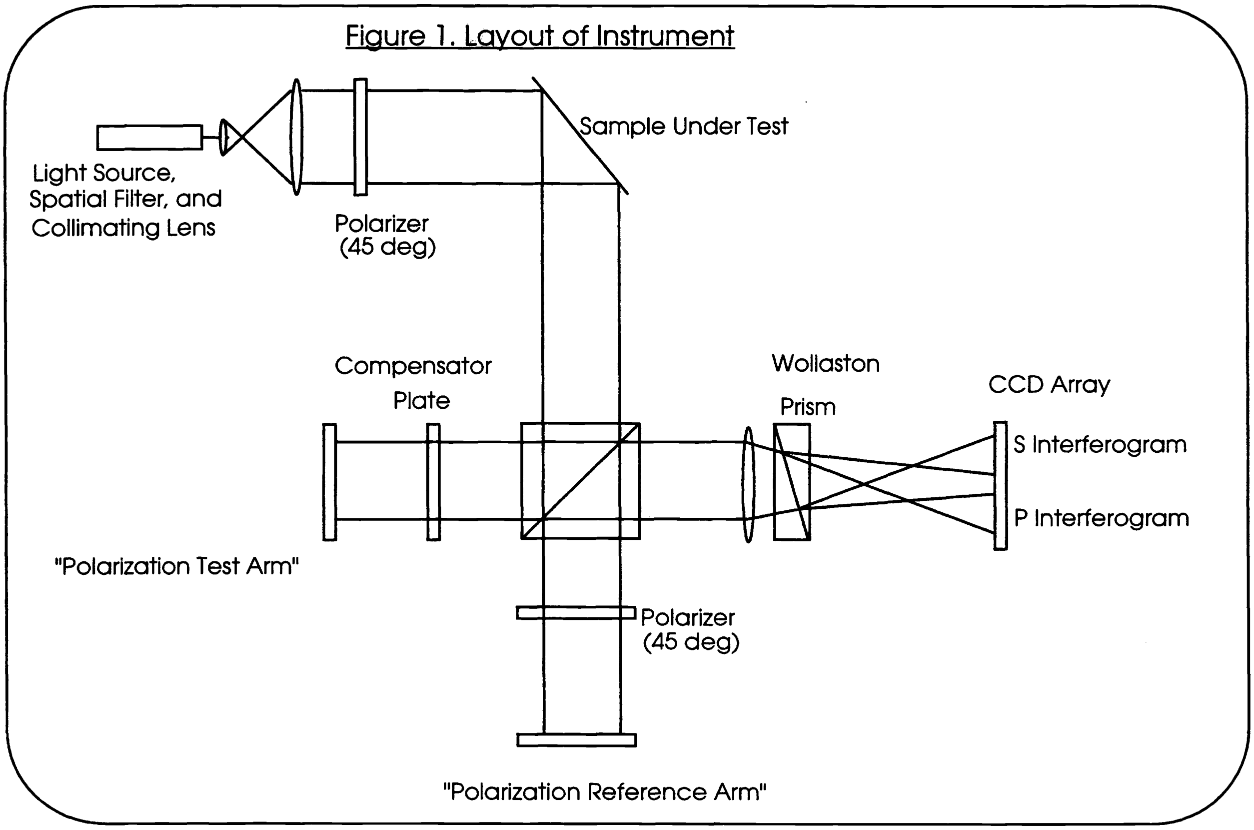

The ellipsometeric parameter Δ is defined as the difference between the P and S phase change on reflection. The ellipsometeric parameter Ψ is defined as the inverse tangent of the ratio of the P and S reflectances.

$$\Delta = P\ Phase - S\ Phase = \Phi_p - \Phi_s \quad \text{Eq. 3}$$

$$Tan\{\Psi\} = \frac{\rho_p}{\rho_s} \quad \text{Eq. 4}$$

The light is directed into the interferometer by a non-polarizing beam splitting cube. This cube is path matched to ensure high contrast fringes when using an incoherent source.

One arm of the interferometer has a polarizer oriented at 45 degrees. This arm can be thought of as a "polarization reference arm" as far as the polarization phase measurement is concerned. This polarizer "scrambles" the polarization phase of the incoming beam by generating a linearly polarized beam from an arbitrarily polarized beam. By definition, a linearly polarized beam has identical phases for the S and P polarizations.

The polarization state of this linearly polarized beam will be compared to the other arm of the interferometer. The electric field returning to the beam splitter from the "polarization reference arm" is

$$E_{reference\ Arm} = \frac{1}{2}\frac{1}{\sqrt{2}}\begin{bmatrix}\rho_s + \rho_p \\ \rho_p + \rho_s\end{bmatrix} e^{i\Phi_{RA}} = \frac{1}{2}C_0\begin{bmatrix}1 \\ 1\end{bmatrix} e^{i\Phi_{RA}} \quad \text{Eq. 5}$$

Where $C_0 = \frac{1}{\sqrt{2}}(\rho_s + \rho_p) = |C_0| e^{i\Phi_{C_0}}$. The term Φ_{RA} represents any polarization independent phase errors due to component imperfection within the reference arm of the interferometer. The ½ and $\sqrt{2}$ come from the amplitude transmittance of the 50/50 beam splitter and the polarizer respectively.

The other arm consists of a compensator plate and return mirror. The compensator is required for incoherent illumination. This arm preserves the phase change on reflection information in the S and P polarization states and can be thought of as the "polarization test arm" for the polarization phase measurement being made. This arm also contains a piezo-electric transducer (PZT) for performing phase shifting interferometry (PSI). Φ_{PSI} represents the phase induced from movement of the PZT while the Φ_{TA} represents the phase errors due to component imperfection in the test arm. The Jones matrix for the beam returning to the beam splitter from the "polarization reference arm" is therefore

$$E_{Test\ Arm} = \frac{1}{2}\begin{bmatrix} \rho_s \\ \rho_p \end{bmatrix} * e^{i(\Phi_{PSI} + \Phi_{TA})} \quad \text{Eq. 6}$$

The beams are recombined and directed through an imaging lens and a Wollaston prism oriented at 0 degrees. The lens images the surface under test onto the CCD camera, while the prism serves to split the S and P polarizations into two distinct interference patterns on the CCD camera. The electric field coming into the Wollaston prism and the resulting interference patterns are:

$$E_{Wollaston\ Prism} = E_{reference\ Arm} + E_{test\ Arm} = \frac{1}{2} C_0 \begin{bmatrix} 1 \\ 1 \end{bmatrix} * e^{i\Phi_{RA}} + \frac{1}{2}\begin{bmatrix} \rho_s \\ \rho_p \end{bmatrix} * e^{i\Phi_{PSI} + \Phi_{TA}} \quad \text{Eq. 7}$$

$$\begin{aligned} I_s &= |E_s|^2 = \left| \frac{C_0}{2} e^{i\Phi_{RA}} + \frac{\rho_s}{2} * e^{i(\Phi_{PSI} + \Phi_{TA})} \right|^2 \\ I_p &= |E_p|^2 = \left| \frac{C_0}{2} e^{i\Phi_{RA}} + \frac{\rho_p}{2} * e^{i(\Phi_{PSI} + \Phi_{TA})} \right|^2 \end{aligned} \quad \text{Eq 8-11}$$

$$I_s = |E_s|^2 = \frac{1}{4}\{C_0^2 + \rho_s^2 + 2\ |C_o|\ |\rho_s|\ Cos\{\Phi_s + \Phi_{PSI} + \Phi_{RA} + \Phi_{TA} + \Phi_{C_0}\}\}$$

$$I_p = |E_p|^2 = \frac{1}{4}\{C_0^2 + \rho_p^2 + 2\ |C_o|\ |\rho_p|\ Cos\{\Phi_p + \Phi_{PSI} + \Phi_{RA} + \Phi_{TA} + \Phi_{C_0}\}\}$$

Phase shifting interferometry[5-7] is used to measure the phase of each interferogram. Phase algorithms involving 3 or more phase steps can be used and are discussed in the above references. The measured phases for the two interferograms are

$$\begin{aligned} Measured\ S\ Phase &= \{\Phi_s + \Phi_{RA} + \Phi_{TA} + \Phi_{C_0}\} \\ Measured\ P\ Phase &= \{\Phi_p + \Phi_{RA} + \Phi_{TA} + \Phi_{C_0}\} \end{aligned} \quad \text{Eq.12-13}$$

Two phenomenon are present in the interference patterns. One is the measurement of component imperfections and polarization phase is the other.

Component imperfections are assumed to be polarization independent and therefore will be the same for the S and P beam. In this way the S and P interferograms are considered to be common path once co-registered and subtracted pixel by pixel. The sum $\Phi_{RA} + \Phi_{TA}$ represents the component imperfections in the interferometer and is common to both interferograms. The phase offset in the reference arm, Φ_{C_o}, is also common to both interferograms.

The only terms that are not common to both interferograms are the S and P phase change on reflection terms. In order to measure the ellipsometeric parameter Δ , the measured P phase is subtracted from the measured S phase.

$$\Delta = P\ Phase - S\ Phase = \Phi_p - \Phi_s . \quad \text{Eq.14}$$

The parameter Ψ can be determined via the visibility of the fringes in the two interferograms. The fringe visibility is defined as γ =(Imax-Imin)/(Imax+Imin). This is identical to the ratio of the AC to DC components of the interference pattern. The visibility of the P and S interferograms can be expressed as:

$$\gamma_p = \frac{\frac{1}{4}\rho_p C_o}{\frac{1}{4}\rho_p{}^2 + \frac{1}{8}C_o{}^2}$$
$$\gamma_s = \frac{\frac{1}{4}\rho_s C_o}{\frac{1}{4}\rho_s{}^2 + \frac{1}{8}C_o{}^2} \quad \text{Eq.15-16}$$

The ratio of the AC components of the visibility yields the ratio of reflectances.

$$Tan\{\Psi\} = \frac{\rho_p}{\rho_s} \quad \text{Eq. 17}$$

Therefore, through the phase and visibility of the two interferograms, this instrument measures the two ellipsometeric parameters.

Two effects have been ignored for clarity. These are the phase change on reflection from the beam splitter coating and the polarization dependant reflections from the beam splitter coating. These are polarization dependent and will therefore affect the Δ and Ψ calculations. Terms representing this effect could be included above and are assumed to be uniform across the aperture. The resulting offsets in Ψ and Δ will be the same for all samples and angles of incidence and their effect can be measured by removing the sample and directing a linearly polarized beam directly into the interferometer. Therefore, the offsets can be measured and removed from subsequent measurements as part of a calibration procedure.

3. Measurements

Measurements of SiO_2 thin films on Si substrates have been made at a range of angles of incidence. Charts 1 and 2 illustrate the measurement of a 51.3nm coating using LED illumination at 644 nm. Charts 3 and 4 illustrate the measurement of a 943nm coating using a HeNe laser. The measurements were made on calibration samples from VLSI Technology of the transition region between the coated and uncoated regions of a silicon wafer. Each chart illustrates the results for the coated and substrate region for a single measurement at multiple angle of incidences.

Figure 2 Delta Characterization for 51.3 nm SiO2 Coating on Si

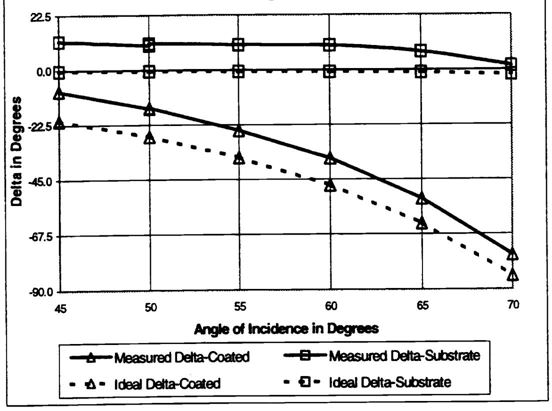

Figure 3. Ratio of Reflectences for 51.3 nm SiO2 Coating on Si

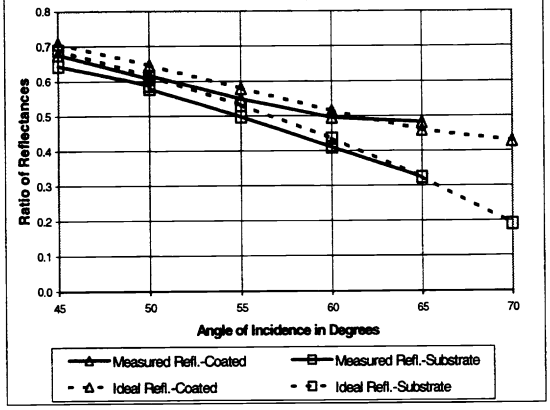

Figure 4. Delta Characterization for 943 nm SiO2 Coating on Si

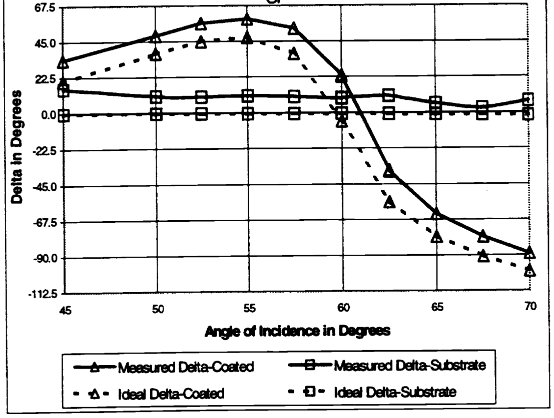

Figure 5. Ratio of Reflectences for 943 nm SiO2 Coating on Si

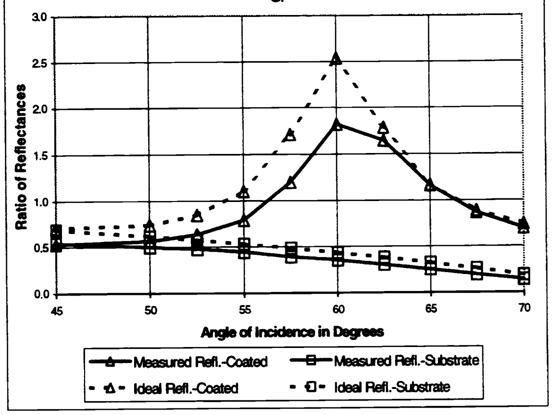

The functional form of the phase change on reflection data agrees well with the theoretical predictions. An offset between the measured and ideal Δ of around 10 degrees can be seen in the plots. This can be attributed to the phase change on reflection from the beam splitter coating and has been confirmed by removing the sample and directing the light directly into the interferometer.

Since the instrument measures the ratio of reflectances directly, ratio of reflectance data ($\mathrm{Tan}(\Psi)$) is plotted rather than Ψ. In this way, constant offsets in the data remain as an offset, whereas if the arc-tangent were used, an offset would no longer be constant. The 51.3 nm ratio of reflectance data functional form is quite good with an average offset to the theoretical data of 0.025. The agreement for the 943 nm coating is not as good. The substrate data has an average offset of 0.088 while the coated data suffers from larger errors that vary with the angle of incidence. At the time of printing, work is under way to determine the source of these errors.

4. Modulation Characterization

The generic form for the intensity of an interference pattern can be represented as

$$I = I_0[1+\gamma \; Cos(\Phi+\Phi_{PSI})] \quad \text{Eq 18}$$

Where I_0 is the average intensity, γ is the fringe modulation (also referred to as fringe visibility), Φ is the phase of the interferogram and Φ_{PSI} is the phase component from the PZT for phase shifting. I_0, γ, and Φ uniquely determine an interference pattern.

Many authors have developed techniques for modulation and average intensity characterization based on various multi-step (3 or more) phase shifting techniques[5-7]. Using phase steps of 0, $\pi/2$, π, and $3\pi/2$ the phase and modulation of a four frame algorithm[7] are

$$\Phi = ArcTan\ [\ \frac{(I_4 - I_2)}{(I_1 - I_2)}\ ]$$

Eq. 19-20

$$\gamma = \frac{\sqrt{[I_4 - I_2]^2 + [I_1 - I_3]^2}}{2I_0} = \frac{2 * \sqrt{[I_4 - I_2]^2 + [I_1 - I_3]^2}}{I_1 + I_2 + I_3 + I_4}$$

Where I_n represents the intensity of the N'th phase step. The modulation is the ratio of the AC to DC components of an interference pattern and it can be shown that the numerator equals ($4\gamma I_0$) and the denominator equals ($4I_0$).

The characterization of the phase and modulation will be perfect if the phase stepping is perfect. In the event that the phase stepping contains errors, the characterization will contain errors. Multi-step techniques have been developed to reduce the errors in the phase characterization and are extremely successful[6]. Each additional step often reduces errors by an order of magnitude. Although techniques for phase error reduction have been developed, literature on modulation error reduction is hard to come by. Because of the large volume of publications involving phase error reduction, the rest of this paper will discuss the reduction of errors in the characterization of the modulation.

Another algorithm uses 5 steps and was developed by Hariharn[7]. It uses steps of $-\pi$, $-\pi/2$ 0, $\pi/2$, and π. The equations can be written

$$\Phi = ArcTan\ [\ \frac{2(I_2 - I_4)}{2I_3 - I_5 - I_1}\ ]$$

Eq. 21-22

$$\gamma = \frac{3\sqrt{4[I_4 - I_2]^2 + [I_1 + I_5 - 2I_3]^2}}{2(I_1 + I_2 + 2I_3 + I_4 + I_5)}$$

The extended averaging technique[6] is used to reduce the errors in the calculation of fringe modulation. The technique acts as a windowing operation through the use of more steps. Given an algorithm using 4 frames of the form

$$\gamma_4 = \frac{N}{D} \quad \text{Eq. 23}$$

Adding one more frame of data a new algorithm can be written as

$$\gamma_{4+1} = \frac{N_1 + N_2}{D_1 + D_2} = \frac{N'}{D'} \quad \text{Eq. 24}$$

Where N_1 (D_1) and N_2 (D_2) represent the numerator (denominator) of the algorithm for frames 1-4 and 2-5 respectively from equation 20. This effectively averages the data for the two sets of frames which are $\pi/2$ apart. Extending this technique to frames 3-5 (4-6) we can write an algorithm for the 4+2 (4+3) algorithm as

$$\gamma_{4+2} = \frac{N'+N''}{D'+D''} = \frac{N_1 + 2N_2 + N_3}{D_1 + 2D_2 + D_3}$$

$$\gamma_{4+3} = \frac{N'+N''+N''+N'''}{D'+D''+D''+D'''} = \frac{N_1 + 3N_2 + 3N_3 + N_4}{D_1 + 3D_2 + 3D_3 + D_4} \qquad \text{Eq. 25-26}$$

This process can continue for as many frames as are desired using this technique and equation 20 for the 4 frame modulation. Using the 4+3 algorithm, it became clear that errors form the denominator of the modulation equation, i.e. the characterization of I_0, are larger than the errors in the numerator.

The Carre' technique[6] calculates the phase between the steps and uses this information to calculate the phase and modulation. Using phase steps of $-3\pi/2$, $-\pi/2$, $\pi/2$ and $3\pi/2$ the equations for the phase between steps, phase and modulation for the Carre' technique are

$$Tan[\frac{\Phi_{PSI}}{2}] = \frac{\sqrt{3[I_2 - I_3] - [I_1 - I_4]}}{\sqrt{[I_2 - I_3] + [I_1 - I_4]}}$$

$$Tan[\Phi] = Tan[\frac{\Phi_{PSI}}{2}] \; [\; \frac{(I_2 - I_3) + (I_1 - I_4)}{(I_2 + I_3) - (I_1 + I_4)} \;] \qquad \text{Eq 27-29}$$

$$\gamma = \frac{\sqrt{[(I_2 - I_3) + (I_1 - I_4)]^2 + [(I_2 + I_3) - (I_1 + I_4)]^2}}{2I_0}$$

The denominator of the modulation equation contains the average intensity I_0. For perfect phase steps $I_0 = (1/4) * [I_1 + I_2 + I_3 + I_4]$. Using equation 18 it can be shown that for an arbitrary phase between steps of Φ_{PSI}:

$$I_1 + I_2 + I_3 + I_4 = I_0[\; 4 + 2\; \gamma\; Cos(\Phi)\; [\; Cos[\frac{\Phi_{PSI}}{2}] + Cos[\; 3\frac{\Phi_{PSI}}{2}]\;]$$

$$I_0 = \frac{I_1 + I_2 + I_3 + I_4}{[\; 4 + 2\; \gamma\; Cos(\Phi)\; [\; Cos[\frac{\Phi_{PSI}}{2}] + Cos[\; 3\frac{\Phi_{PSI}}{2}]\;]} \qquad \text{Eq. 30-31}$$

Equation 31 provides for the calculation of I_0 in the presence of phase shifter miscalibration. It requires the calculation of the phase between steps, the phase of the interferogram and the modulation to calculate I_0. The Carre' technique can provide the phase between steps but suffers from errors when the phase of the interference pattern is a multiple of π. An algorithm[9] developed by Wyant and Cheng can also be used to determine the phase between steps.

$$Cos[\Phi_{PSI}] = \frac{1}{2}\frac{I_1 - I_5}{I_2 - I_4} \qquad \text{Eq 32}$$

This algorithm suffers from errors at $3/4\pi + N\pi$. Figure 6 illustrates the performance of the two phase step calculating algorithms for a 5% non linear phase shifter error. In this case the average phase step is actually 86.6 degrees. Given a linear and non linear phase stepping error of α_{linear} *and* $\alpha_{nonlinear}$ the motion of the phase stepper is modeled as

$$Linear\ PSI\ Steps\ \Phi_{PSI} = \Phi_{PSI\ linear} = \frac{\pi}{2} * (1 + \alpha_{linear})$$

Eq. 33-34

$$Non-Linear\ PSI\ Steps\ \ \Phi_{PSI} = \Phi_{PSI\ nonlinear} = \frac{\pi}{2} * [1 + \alpha_{nonlinear}\Phi_{PSI\ linear} - \alpha_{nonlinear}]$$

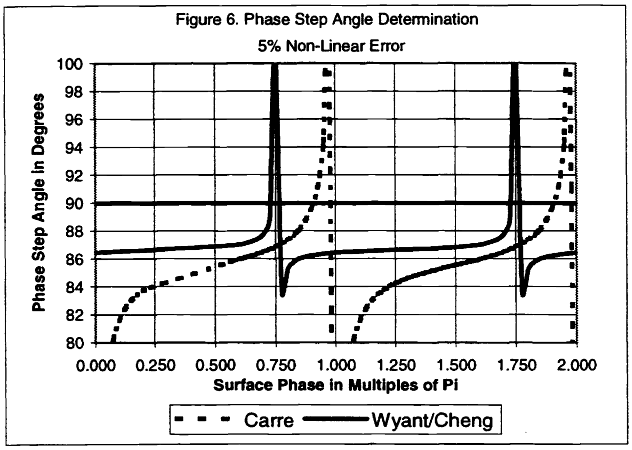

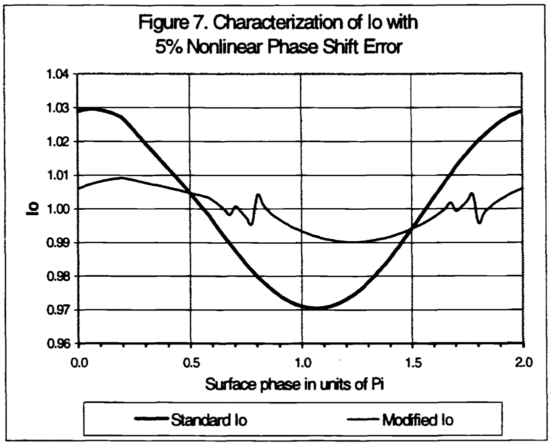

The Wyant/Cheng algorithm is superior over most of the surface phase values. The Carre algorithm can be used near surface phases of $3/4\pi + N\pi$ to obtain an algorithm that minimizes the errors over the entire range.

The average intensity (equation 31) requires knowledge of the surface phase and modulation. The surface phase characterization is measured by using a 4+3 algorithm[6], the errors in which are negligible. The modulation will also be characterized using the 4+3 algorithm as a first order approximation for use in the average intensity equation. A modified version of the 4+3 algorithm will use the numerator of the 4+3 modulation equation in conjunction with the average intensity calculation in the denominator. Figure 7 illustrates two average intensity algorithms. The standard equation is the sum of four frames while the second uses equation 31 with 4+3 phase and modulation data. There is a factor of 3 improvement in the characterization of I_o.

Figures 8-9 illustrate the peak error in reflectance ratio calculation due to phase shift calibration error. Five separate algorithms are plotted. The Harihthe and four others based on the four step technique using 5, 6 and 7 frames. Except for the last one they all use the standard denominator for their algorithm. The one labeled "4+3 w/ Special I_o" uses the I_o calculation from equation 31.

The use of the modified I_o calculation in the denominator of the modulation calculation reduces the error in the calculation from 1.68% to 0.47% for a linear calibration error of –5%. The improvement in the nonlinear case is only 0.12%. In the case of a nonlinear error of +5% the numerator and denominator of the 4+3 algorithm are in error by 0.12% and 2% respectively. The modified I_0 calculation is in error by 1.91%. This is a minimal improvement and it is the characterization of I_0 (denominator of modulation equation) that causes the errors in the modulation characterization. More work will be required to improve the I_o calculation.

The imaging ellipsometer requires the AC component of the visibility to calculate the ratio of reflectance and the errors in this component are much smaller. The maximum error for the numerator of a 4+3 frame algorithm for a 5% linear and nonlinear error are 0.38% and 0.22% respectively. The magnitude of the errors seen in figures 2-5 is too large to be attributed to phase shifter errors.

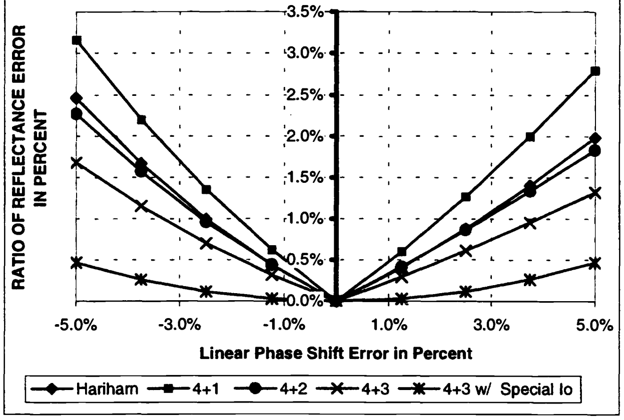

Figure 8. Peak Error In Reflectance Ratio Error Due to Linear Phase Shift Calibration Error

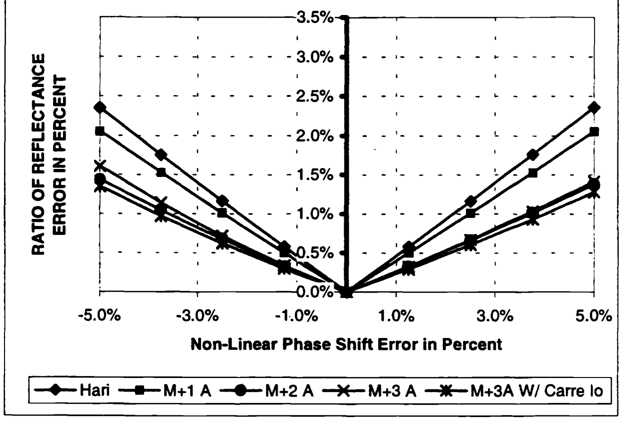

Figure 9. Peak Error In Reflectance Ratio Error Due to Non-Linear Phase Shift Calibration Error

5. Conclusion

The theory of a new imaging phase shifting ellipsometer has been presented. Results from a prototype instrument indicate good agreement to theory. Future work will concentrate on the reduction of systematic errors and calibration techniques.

Results of new algorithms for the characterization of fringe modulation have been presented. These greatly reduced the errors due to linear calibration errors, and were marginally successful for nonlinear errors. The characterization of the average intensity of the interferogram is the largest contributor to the errors in the modulation. More work will be required to reduce these errors.

References

1) Hazebroek H F and Holscher A A 1973 "Interferometeric ellipsometry" *J. Phys. E: Sci. Instrum.* **6** 822-826
2) Lin C, Chou C and Chang K, 1990 "Real time interferometric ellipsometry with optical heterodyne and phase lock in techniques" Applied Optics V 29 #34 pp5159-5162
3) Cohn R. F., Wagner J W, Kruger J 1988 "Dynamic imaging microellipsometry: theory, system design, and feasibility demonstration" Applied Optics V 27(22) pp4664-4671 November 15, 1988
4) Mishima T, Kao K C 1982 "Detection of thickness uniformity of film layers in semiconductor devices by spatially resolved ellipsometry" Optical Engineering Col 21(6) pp1074-1078 Nov/Dec 1982
5) Creath, K "Phase measurement interferomety techniques" in Progress in Optics XXVI. E. Wolf editor Elsevier Science Publishers 1988
6) Schmit, J, Creath K, 1995 "Extended averaging technique for derivation of error-compensating algorithms in phase shifting interferomety" Applied Optics Vol 34(19) pp3610-3619
7) J. E. Grievenkamp and J H Brunning, "Phase Shifting Interferometry" Ch 14 in Optical Shop Testing, Second Edition, Ed D. Malacara 1992 John Wiley and Sons
8) Wells, C 1997 "Fringe modulation characterization for a phase shifting imaging ellipsometer" SPIE Proceeding vol 3134-51
9) Y-Y Cheng, and J C Wyant, "Phase Shifter Calibration" Applied Optics Vol 24 (18) 15 September 1985